Effect of the Disulfide Bridge and the C-Terminal Extension on the Oligomerization of the Amyloid Peptide ABri Implicated in Familial British Dementia†

Omar M. A. El-Agnaf,*,‡ Joseph M. Sheridan,‡ Christina Sidera,‡ Giuliano Siligardi,§ Rohanah Hussain,§ Parvez I. Haris,|| and Brian M. Austen*,‡

Neurodegeneration Unit, Department of Surgery, St. George's Hospital Medical School, Cranmer Terrace, Tooting, London SW17 0RE, U.K., Department of Pharmacy, King's College, Franklin-Wilkins Building, 150 Stamford Street, London SE1 8WA, U.K., and Department of Biological Sciences, De Montfort University, The Gateway, Leicester LE1 9BH, U.K.

Received September 28, 2000; Revised Manuscript Received January 9, 2001

ABSTRACT: Familial British dementia (FBD) is a rare neurodegenerative disorder and shares features with Alzheimer's disease, including amyloid plaque deposits, neurofibrillary tangles, neuronal loss, and progressive dementia. Immunohistochemical and biochemical analysis of plaques and vascular amyloid of FBD brains revealed that a 4 kDa peptide named ABri is the main component of the highly insoluble amyloid deposits. In FBD patients, the ABri peptide is produced as a result of a point mutation in the usual stop codon of the BRI gene. This mutation produces a BRI precursor protein 11 amino acids longer than the wild-type protein. Mutant and wild-type precursor proteins both undergo furin cleavage between residues 243 and 244, producing a peptide of 34 amino acids in the case of ABri and 23 amino acids in the case of the wild-type (WT) peptide. Here we demonstrate that the intramolecular disulfide bond in ABri and the C-terminal extension are required to elongate initially formed dimers to oligomers and fibrils. In contrast, the shorter WT peptide did not aggregate under the same conditions. Conformational analyses indicate that the disulfide bond and the C-terminal extension of ABri are required for the formation of β-sheet structure. Soluble nonfibrillar ABri oligomers were observed prior to the appearance of mature fibrils. A molecular model of ABri containing three β-strands, and two β-hairpins annealed by a disulfide bond, has been constructed, and predicts a hydrophobic surface which is instrumental in promoting oligomerization.

Familial British dementia (FBD)[1] is a rare autosomal dominant neurodegenerative disorder that shares features of Alzheimer's disease (AD), including amyloid plaques surrounded by astrocytes and microglia, neurofibrillary tangles, neuronal loss, and progressive dementia (*1*, *2*). It is clinically characterized by the onset of dementia in the fifth decade, progressive spastic tetraparesis, and cerebellar ataxia. FBD is distinguished from AD and other dementing disorders by plaque deposition in the cerebellum and the accompanying cerebellar ataxia. This condition has previously been reported as an atypical form of familial AD (*3*). Histological studies show that amyloid deposits in FBD patients exhibit yellow-green birefringence under polarized light after staining with Congo Red, indicating the presence of amyloid-like fibrils with β-sheet structure (*4*). Immunohistochemical and biochemical analysis of plaques and the vascular amyloid of FBD brains revealed that a 4 kDa peptide named ABri is the main component of the highly insoluble amyloid deposits likely to be involved in FBD pathogenesis (*4*).

The ABri peptide was determined to be a fragment derived from a larger, membrane-anchored precursor protein, termed the BRI precursor protein, and encoded by the *BRI* gene on chromosome 13 (*4*). The wild-type BRI protein has 266 amino acid residues, whereas FBD patients have a single nucleotide transition (T → A) that converts the stop codon (TGA) into AGA. This mutation changes the length of the BRI precursor protein to 277 amino acids (*4*). Furin-mediated endoproteolytic processing of mutant BRI between Arg243 and Glu244 produces the 34-residue carboxy-terminal fragment, the ABri peptide (*5*). Cells transfected with the wild-type or mutant BRI gene were found to produce ∼3 or ∼4 kDa peptides corresponding to the cleaved WT peptide or ABri, respectively (*5*). Notably, the cells transfected with the mutant BRI produced more peptide than those transfected with the wild type, indicating that the carboxy-terminal extension enhances furin proteolysis (*5*).

The appearance of ABri in the pathological lesions found in regions of the central nervous system most affected in FBD implicates its accumulation in the pathogenesis of FBD. However, the role(s) of ABri in the pathogenesis of FBD is

† This work was supported by funding from the UK Medical Research Council and CeNeS plc.

* To whom correspondence should be addressed: Neurodegeneration Unit, Department of Surgery, St. George's Hospital Medical School, Cranmer Terrace, Tooting, London SW17 0RE, U.K. Phone: (20)-8725-5650 or (20)-8725-5650. Fax: (20)-8725-3594. E-mail: oelagnaf@sghms.ac.uk or sghk200@sghms.ac.uk.

‡ St. George's Hospital Medical School.

§ King's College.

|| De Montfort University.

[1] Abbreviations: AD, Alzheimer's disease; Aβ, β-amyloid protein; ABri, British amyloid; ADan, Danish amyloid; DMSO, dimethyl sulfoxide; FBD, familial British dementia; FTIR, Fourier transform infrared; HFIP, 1,1,1,3,3,3-hexafluoro-2-propanol; HPLC, high-pressure liquid chromatography; PAGE, polyacrylamide gel electrophoresis; SEC, size exclusion chromatography; WT, wild-type.

10.1021/bi002287i CCC: $20.00
Published on Web 03/02/2001

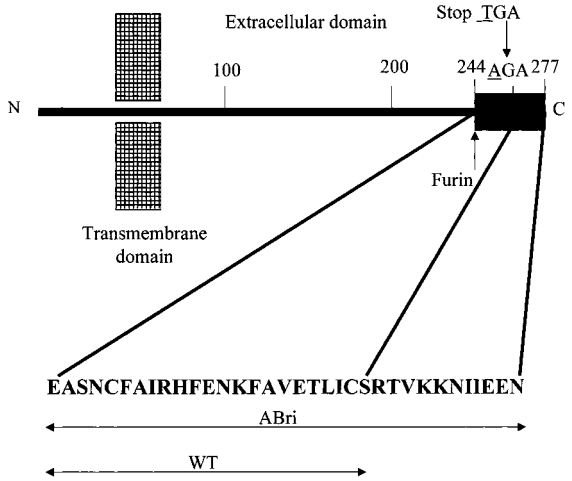

FIGURE 1: Schematic presentation of the amyloid precursor protein and amyloid peptide ABri in patients affected with FBD. A single-base substitution at the stop codon of the BRI gene (Stop267 → Arg) in patients with FBD generates a longer reading frame, and a larger 277-residue transmembrane protein precursor molecule. The arrows indicate the furin cleavage site of the precursor proteins between codons 243 (Arg) and 244 (Glu) that produce the WT and ABri peptides.

unknown. Understanding the pathogenesis of the FBD may shed light on the cause of dementia in AD as well as in other neurodegenerative disorders related to protein aggregation (reviewed in refs *6*−*8*). Here we report the novel findings that the intramolecular disulfide bond in ABri and the C-terminal extension are required for ABri oligomeriztion and the formation of amyloid-like fibrils. Furthermore, circular dichroism (CD) and Fourier transform infrared (FTIR) conformational analysis indicates that the C-terminal extension of ABri and the disulfide bond are required for the formation of β-sheet structure in ABri aggregates. A molecular model of ABri containing three β-strands and two β-hairpins and annealed by a disulfide bond has been constructed, which predicts a hydrophobic surface which may be instrumental in promoting oligomerization.

EXPERIMENTAL PROCEDURES

Peptide Synthesis. An Fmoc/tBu methodology, optimized for amyloid peptides, was used (*9*) on a Milligen 9050 peptide synthesizer (PE Applied Biosystems Ltd., Cheshire, U.K.) with Ser-PEG-PS and Asn-PEG-PS resins (0.2 mmol) for WT and ABri peptides, respectively (the sequences of the ABri and WT peptides are shown in Figure 1). Peptides were purified using reversed phase HPLC, with solvent gradients of 0.1% TFA and a 0.1% TFA/acetonitrile mixture (v/v). Analytical HPLC was performed on a Phenomenex Jupiter C4 column (250 mm × 4.6 mm), while preparative HPLC was carried out on a Vydac C4 (250 mm × 22 mm) 214TP1022 column. The purity of the peptides was judged to be greater than 95% by analytical HPLC. Electrospray mass spectrometry confirmed the desired products (see below).

Peptide Oxidation. Lyophilized peptides were dissolved (0.1 mg/mL) in 0.1 M ammonium bicarbonate at pH 8.0. The reaction mixture was stirred overnight at room temperature. The oxidation was monitored by analytical HPLC which showed the disappearance of the reduced peptide peak and the concurrent emergence of the cyclic peptide peak. Peptides were lyophilized and then purified using preparative HPLC (see above). Cyclization was confirmed by electrospray mass spectrometry, which showed the loss of 2 mass units from the cyclic peptide compared to the reduced peptide. Electrospray mass spectrometry confirmed the expected average MW of the products: reduced ABri peptide (red-ABri), calculated (average MW) 3955.56, found 3955.5; oxidized ABri peptide (ABri), calculated 3953.55, found 3953.7; reduced WT peptide (red WT), calculated 2630.02, found 2629.23; and oxidized WT peptide (WT), calculated 2628.00, found 2627.43. Aged solutions of ABri or WT (5 mg/mL) in sterile 0.1 M Tris-HCl (pH 9) were prepared by incubation at 37 °C for 3 weeks. MS/MS of WT nanosprayed in 5% methanol in a Termoquest LCQ mass spectrometer gave a peak at *m*/*z* 1752, from the triply charged dimer at 5254 amu, which was trapped as a parent ion, disintegrated to the singly charged and doubly charged monomer (*m*/*z* 2627 and 1314). MS/MS of ABri nanosprayed in 5% methanol gave a peak at *m*/*z* 1681, from the quintuply charged dimer ion of 7906 amu, which was trapped as a parent ion, and disintegrated to the triply charged monomer at *m*/*z* 1318.

Gel Electrophoresis. Samples were electrophoresed on precast 16.5% Tris-Tricine gels (Bio-Rad). Fresh and aged samples were diluted 1 part of sample with 2 parts of sample buffer [40% (w/v) glycerol, 2% (w/v) SDS, 0.2 M Tris-HCl (pH 6.8), and 0.005% (w/v) Coomassie G-250]. The concentration of Coomassie G-250 was reduced 10-fold from that recommended by the gel manufacturers, and its comigration with the low-molecular weight peptides obstructed their visualization after staining of the gel. Samples were either not boiled or boiled for 5 min at 80 °C. The gels were loaded with peptide samples, and run in Tricine buffer [1.31% (w/v) Tris base, 1.8% (w/v) Tricine, and 0.1% (w/v) SDS], at 20 mA per gel on the BioRad Mini-Gel. The gels were fixed and stained in 40% (v/v) methanol, 10% (v/v) acetic acid solution containing 0.1% (w/v) Coomassie blue R-250 for 5 h. Destaining was performed in the methanol/acetic acid solution lacking Coomassie blue.

Congo Red Birefringence. Aged 100 μL aliquots of WT or ABri solutions were added to 900 μL of Congo Red solution [2.5 mg/100 mL in PBS (pH 7.4)]. This mixture was incubated for 1 h at room temperature and then centrifuged. The resultant pellet was placed on a slide and examined under polarizing light using an Nikon Optiphot light microscope under a 10× lens.

Congo Red Binding. Congo Red (20 μM) in PBS (pH 7.4) was prepared and filtered through a 0.45 μm cellulose acetate filter. Aliquots (40 μL) of the aged peptide solution were incubated with Congo Red (960 μL) at room temperature for 30 min, and absorption spectra between 400 and 600 nm were collected with a Jasco V-530 spectrophotometer.

Electron Microscopy. Electron micrographs were produced from aged peptide solutions. The samples were fixed with glutaraldehyde, stained with uranyl acetate, and examined on a Zeiss 900 TEM instrument (*10*).

Size Exclusion Chromatography (SEC) System. At various time points, aliquots (20 μL) of ABri or WT peptides incubated at 5 mg/mL in 0.1 M Tris-HCl (pH 9) were loaded on a Superdex 75 column (10 mm × 270 mm) and eluted with 0.1 M Tris-HCl (pH 9) at a flow rate of 0.5 mL/min. The eluate was monitored at 215 nm.

Circular Dichroism (CD) Spectroscopy. Spectra were recorded using nitrogen-flushed JASCO J720 and J600 spectropolarimeters, and scans were obtained using a time constant of 4 s, a scan speed of 10 nm/min, and a spectral bandwidth of 2 nm. Both spectropolarimeters were calibrated with ammonium D-camphor-10-sulfonate. Quartz cells of 0.02 and 1 cm were used for measurements in the far-UV (185−250 nm) and near-UV (250−350 nm) regions, respectively. CD spectra were reported as $\Delta\epsilon = \epsilon_L - \epsilon_R$ (M^{-1} cm^{-1}) based upon an average molecular weight per amino acid of 113. UV spectrophotometry was used to determine the absolute concentration of peptides from calculated extinction coefficients in solution to calculate the differential molar extinction coefficient $\Delta\epsilon$.

Fourier Transform Infrared (FTIR) Spectroscopy. Infrared spectra were recorded at 25 °C using a Nicolet FTIR spectrometer continuously purged with dry air. Samples were placed in a 10 mL gastight CaF_2 cell with a 50 mm path length. One thousand scans were signal averaged at a resolution of 4 cm^{-1}. The analysis of the amide I band was carried out using a second-derivative procedure (*11*, *12*). Second-derivative spectra were calculated using the OMNIC software Derivative function with a 13-data point Savitzy−Golay smoothing window.

Molecular Modeling of ABri. Molecular modeling was performed on Swiss-PdbViewer (SPDBV) (*13*) and SYBYL version 6.1 (TRIPOS Inc.). Using the crystal structure of transthyritin (*14*) as a template (1BM7), Glu1−Cys22 of ABri were modeled onto Gly101−Val122 of 1BM7 which contained a long β-hairpin with a type I β-turn. The C-terminal β-turn of ABri was templated on the type I β-turn of Ser112−Ser115 in 1BM7. This turn and a C-terminal β-strand were manually fitted to the initial hairpin, optimizing backbone hydrogen bonding and side chain interactions. Using SYBYL, the disulfide bond was formed and any breaks in the backbone were mended. Side chain rotamers were then optimized in SPDBV, satisfying interstrand interactions where appropriate (*15*). The structure was relaxed in SYBYL with 100 steps of steepest descents, followed by 200 steps of conjugate gradient minimization, using the Kollmann united atom force field and charges, and the default distance-dependent dielectric. The model was rechecked using the WHAT_CHECK program on the UK EMBL-EBI server (*16*, *17*). The overall twist of the modeled β-sheet is arbitrary and biased by the 1BM7 template.

RESULTS

An Intramolecular Disulfide Bond in ABri. The two cysteines in the peptide sequence of ABri led us to consider the possibility of disulfide bond formation. The reported molecular weights (3935.5) of ABri isolated from FDB brain or transfected cells (*4*) agreed exactly with the formation of an intramolecular disulfide bridge and cyclization of the N-terminal glutamyl residue to pyroglutamyl. Furthermore, tryptic fingerprinting and mass spectrometry have indicated the presence of a disulfide bond in ABri or WT produced by cells transfected with the mutant or wild-type BRI gene, respectively.[2] However, circulating forms of ABri do not contain the N-terminal modification.[3] Therefore, we synthesized the reduced forms of the ABri and WT peptides, and using simple air oxidation at pH 8, we also synthesized the disulfide-bonded forms of the ABri and WT peptides. All had N-terminal glutamyl residues. The reaction was rapid, and disulfide-bonded peptides were readily purified in high yield. This facile synthesis suggests that ABri can readily adopt a disulfide-bonded form. In studies of reduced forms of the ABri or WT peptide, only freshly prepared solutions were used to ensure that only reduced forms were assessed. Aged solutions were prepared from the oxidized forms of the ABri and WT peptides.

Oligomers Were Detected in ABri but Not in WT Solutions. We found that ABri was soluble in Tris-HCl at pH ≥8 (i.e., gave an optically clear solution by eye), but less soluble at pH 7.4. Thus, we prepared all stock peptides in 100 mM Tris-HCl (pH 9) at 5 mg/mL unless otherwise noted. To examine possible self-aggregation of WT and ABri, we aged solutions at 5 mg/mL for 3 weeks and analyzed them using SDS−PAGE, performed in the presence or absence of the reducing agent DTT. A series of oligomers with increasing molecular weights were detected in both fresh and aged solutions of ABri without DTT (Figure 2A); sample treatment by boiling did not affect the appearance of these bands (Figure 2A). Aggregated ABri species were found near the interface with the stacking gel in aged but not in fresh samples, suggesting the formation of larger aggregates that did not enter the separating gel (Figure 2A). Under the same conditions, a comparable series of oligomers of increasing size were not detected in fresh or aged WT samples (Figure 2A). Interestingly, when ABri samples were treated with DTT, the aggregates disappeared (Figure 2B). This evidence supports the important role of the disulfide bridge in ABri oligomerization.

The most predominant low-molecular weight species in ABri solutions migrated between the 4000 and 8000 molecular weight markers, indicating that it might have been a dimer (Figure 2). Similarly, the only species detected in WT solutions migrated as a dimer. The presence of dimers in aqueous solutions of WT and ABri was confirmed by electrospray MS, which showed the presence of a triply charged species of the WT dimer, at *m*/*z* 1752, and the presence of a quintuply charged ion of the ABri dimer at *m*/*z* 1581. Subsequently, both were identified by the fragments produced by MS/MS of the trapped ions. These species containing odd numbers of charges could not have been formed from monomers. No oligomeric species were detected in freshly prepared solutions of red-ABri or red-WT (data not shown). When the same solutions of ABri and WT were subjected to SEC, only a single dimer peak was detected in the freshly prepared or aged solutions of WT (see below). Freshly prepared ABri produced a large dimer peak, and a small peak eluted in the void volume of the column (Figure 3). When the ABri sample was aged for 3 weeks, only the void peak was observed (Figure 3).

Congo Red Exhibits an Amyloid-Characteristic Absorption Shift and Birefringence upon Binding to Fibrillar ABri. One of the distinguishing features of amyloid fibrils is their ability to bind the Congo Red dye commonly used to stain amyloid in tissue sections (*18*−*20*). Congo Red bound to ABri fibril

[2] S. S. Sisodia, personal communication.

[3] J. Ghiso, personal communication.

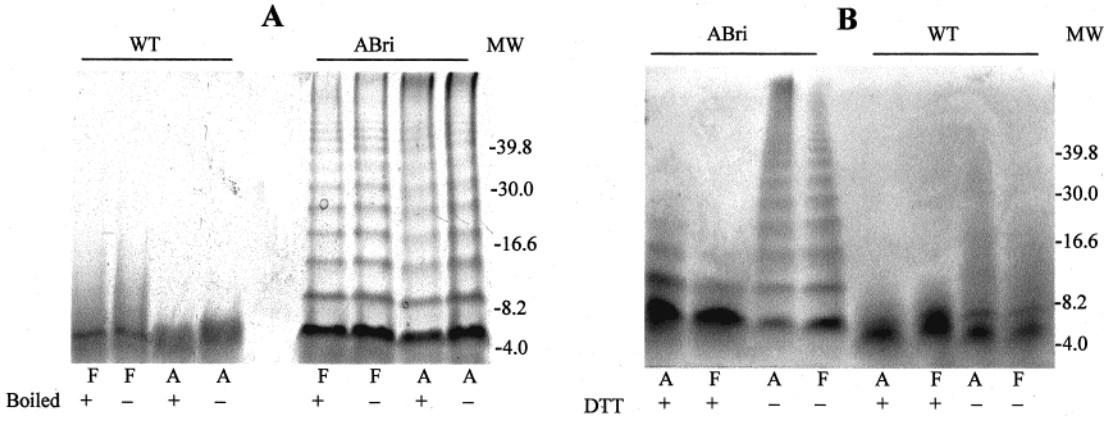

FIGURE 2: SDS−PAGE analysis of the self-oligomerization of fresh and aged ABri and WT peptides. Aged (A) and fresh (F) solutions of the peptides were prepared, as described in Experimental Procedures, and analyzed by SDS−PAGE after boiling in the presence of DTT (B lanes 1, 2, 5, and 6) or in the absence of DTT (A lanes 1, 3, 5, and 7) or incubating in sample buffer without DTT at room temperature (A lanes 2, 4, 6, and 8; and B lanes 3, 4, 7, and 8). Extensive self-oligomerization was observed only in ABri samples without DTT. High-molecular weight aggregates that did not penetrate the separating gel were detected in the aged sample of ABri without DTT (A lanes 7 and 8 and B lane 3). Peptides (150 nmol) were loaded on the gel except that there was 200 nmol of WT each in B lanes 5−8.

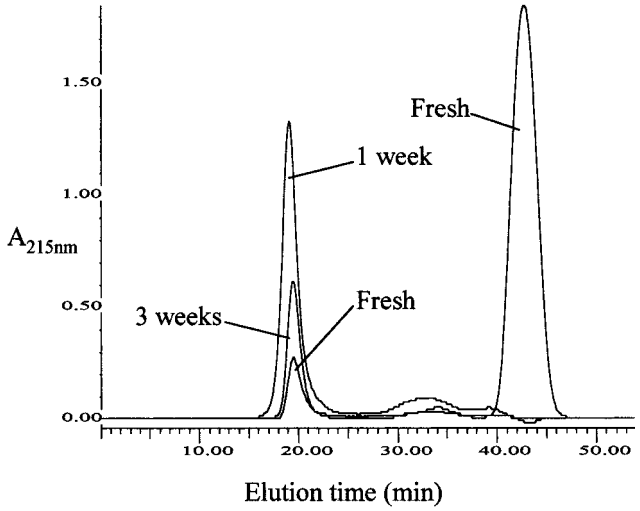

FIGURE 3: Size exclusion chromatography of ABri. A freshly prepared solution of ABri (5 mg/mL) in 0.1 M Tris-HCl (pH 9) buffer was fractionated on a Superdex 75 column after incubation for 0, 1, and 3 weeks at 37 °C. The gel-included peak elutes at ~42.34 min, while the gel-excluded peak elutes at ~19.4 min.

and, produced characteristic intense yellow-green birefringence, when observed under a polarizing microscope (Figure 4A,B). As a positive control, the Congo Red-induced birefringence produced from Aβ40 fibrils is also shown (Figure 4C,D). In contrast, Congo Red did not bind to the aged WT solution prepared under the same conditions as ABri. A shift in the absorption spectrum of Congo Red to longer wavelengths, upon binding to amyloid fibrils, has been described (*21*, *22*, and references therein). A similar spectral shift from a λ_{max} of 487 nm to a λ_{max} of 496 nm was observed upon incubation of ABri fibrils with Congo Red (Figure 5). This spectral shift was not observed for aged WT under the same conditions, indicating the absence of fibrils in the WT sample.

ABri Forms Typical Amyloid-like Fibrils. We used EM to examine uranyl acetate-stained preparations, made from peptide solutions that were either fresh or aged under the conditions described above. Long, intertwined fibrils of variable length and 5−9 nm in diameter were seen in aged samples of ABri (Figure 6A), whereas fibrils were not detected in fresh samples. Under the same conditions, fibrils were not detected in fresh or aged samples of the WT peptide.

Protofibrils of ABri Were Separated from Dimers and Mature Fibrils. After incubation for 3 weeks, an ABri solution was subjected to SEC (*23*). The void volume peak containing high-molecular weight oligomers was collected and examined by electron microscopy. Short curly fibrils 2.5−8.5 nm in diameter and 10−60 nm in length on average (Figure 6B) were observed. Elongated protofibrils or mature fibrils were not detected. These structures are similar to protofibrils formed by Aβ and α-synuclein; thus, to distinguish them from mature ABri fibrils, we refer to them as protofibrils.

Kinetics of Protofibril Formation. The rates of oligomerization in ABri and WT solutions were compared by SEC (*23*). Immediately after dissolution, ABri produced a single chromatographic peak with a retention time equivalent to that of a dimer. The area of this ABri peak declined drastically by ~100% over 7 days. In contrast, although WT produced a peak with a retention time equivalent to that of a dimer, the area of this peak declined only <5% over the course of 3 weeks. The peak area of protofibrils formed by ABri increased rapidly within the first week. However, in the second and third weeks, the protofibril peak height decreased (Figure 7). For ABri, this initial formation and subsequent decline in the protofibril peak area are consistent with the protofibril being an intermediate in the pathway to ABri insoluble fibrils. In contrast, WT exhibited only a dimer peak which did not change as incubation was prolonged, and no higher-molecular weight peak was detected, consistent with the absence of aggregates (Figure 7).

Circular Dichroism (CD) and Fourier Transform Infrared (FTIR) Spectroscopy Indicated That ABri Contains More β-Sheet Structure Than WT. FTIR and CD spectroscopy were used to characterize the conformation of ABri and WT peptides. The ABri peptide was soluble in H_2O at pH 4.3 or ≥8 (i.e., gave an optically clear solution by eye), at concentrations between 1 and 5 mg/mL. The peptide precipitated at intermediate pH values. In contrast, the solubilities of red-ABri, WT, and red-WT were not pH-dependent.

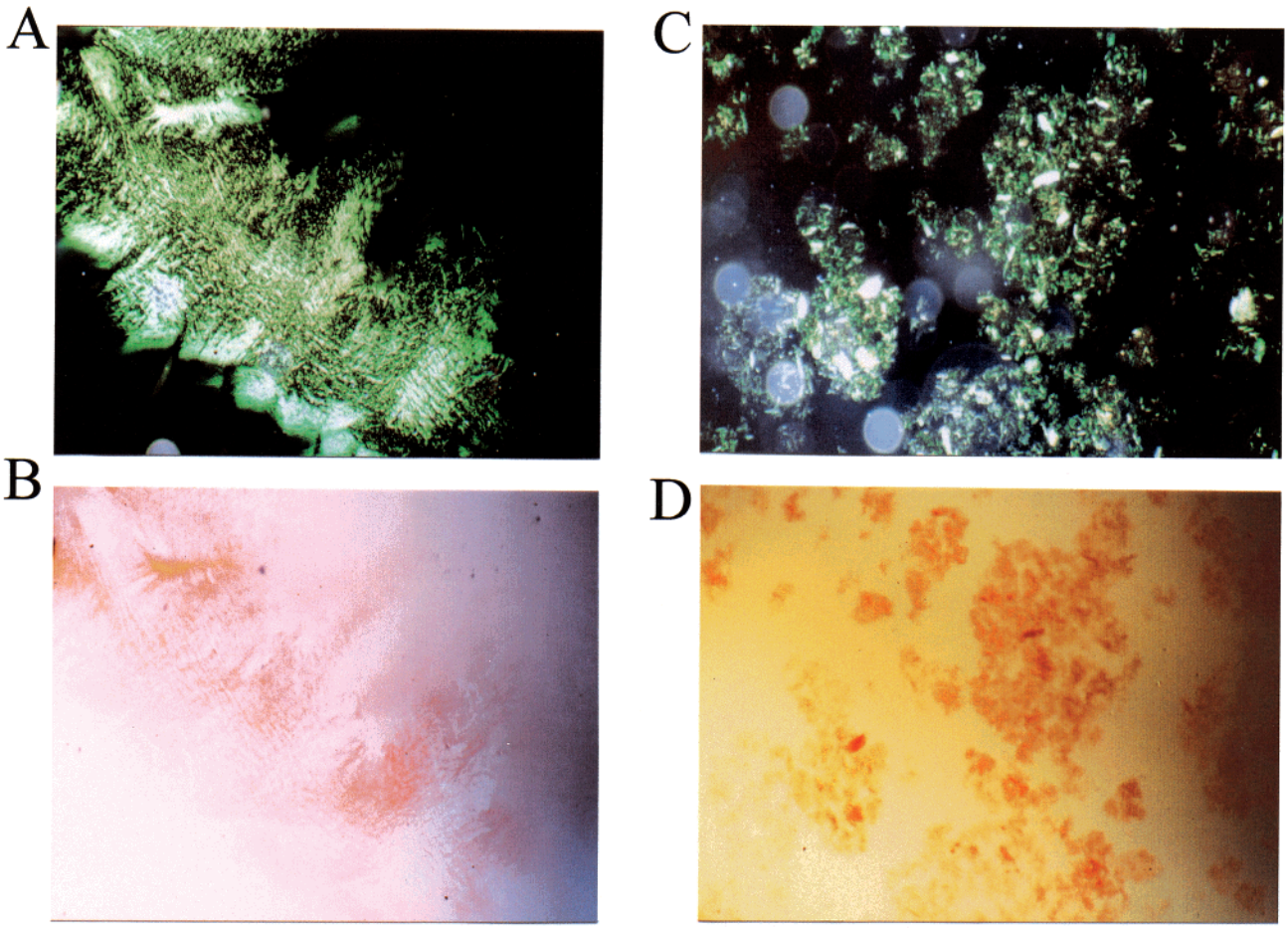

FIGURE 4: Birefringence of Congo Red-stained ABri and Aβ40 fibrils. Panels A and C show birefringent staining observed through a polarized filter: (A and B) ABri fibrils and (C and D) Aβ40 amyloid fibrils. The polarizer orientations in panels A and C were perpendicular to those in panels B and D.

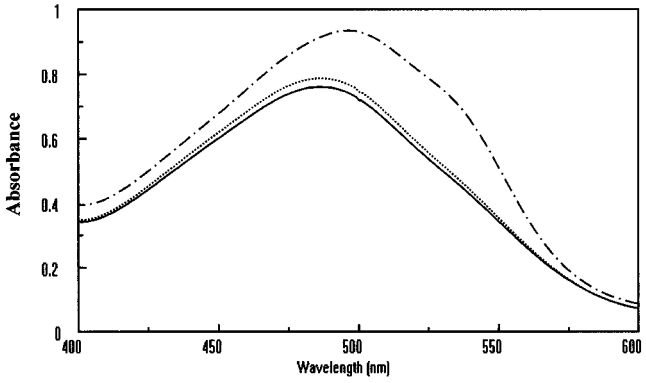

FIGURE 5: Comparison of Congo Red binding to aged ABri and WT solutions. Peptide (5 mg/mL) solutions in 0.1 M Tris-HCl (pH 9) buffer were aged for 3 weeks and then tested for Congo Red binding. Congo Red binding to ABri fibrils shifts the absorbance spectra of Congo Red: Congo Red (—), Congo Red incubated with ABri fibrils (—•—), and Congo Red incubated with an aged WT solution (•••).

CD Measurements. The effects of aging on the secondary structure of WT and ABri peptides in both backbone (far-UV, 185−250 nm) and aromatic/disulfide (near-UV, 250−330 nm) regions were studied. Peptide solutions were prepared in 100 mM Tris-HCl (pH 9) at 5 mg/mL and diluted 10-fold immediately before CD spectroscopy.

Freshly prepared dilutions of ABri in 100 mM Tris-HCl (pH 9) generated a CD spectrum with a maximum at 190 nm and a minimum at 210 nm (Figure 8A), characteristic of a β-sheet. After incubation for 3 weeks, the minimum shifted to 216 nm and the intensity of the CD curves increased, indicative of an increase in β-sheet content (Figure 8A). In contrast, CD curves from a freshly prepared red-ABri solution gave spectra with a minimum at 200 nm, characteristic of irregular structure (random conformation; data not shown).

The CD spectrum of freshly prepared solutions of red-WT or WT exhibited random coil conformation with a minimum at 200 or 203 nm, respectively, whereas after incubation for 3 weeks, the CD spectra of WT indicated a conversion to some β-sheet with a minimum at 208 nm (Figure 8A).

The appearance of a positive CD band centered about 240 nm and changes between 250 and 270 nm in the aged ABri solution indicated conformational changes affecting the microenvironments of the disulfide and/or phenylalanine residues (Figure 8A).

A titration from pH 4 to 9 on freshly prepared solutions revealed CD spectral changes that differentiate and discriminate between the oxidized ABri and WT forms. All peptides at low pH ($\leq$4) exhibited a CD spectrum with a minimum at 200 nm characteristic of random coil. The CD spectra of the reduced forms of ABri and WT exhibited more intense negative bands, consistent with more irregular conformation compared to the oxidized forms (data not shown). However, only ABri exhibited a random coil to β-sheet transition when

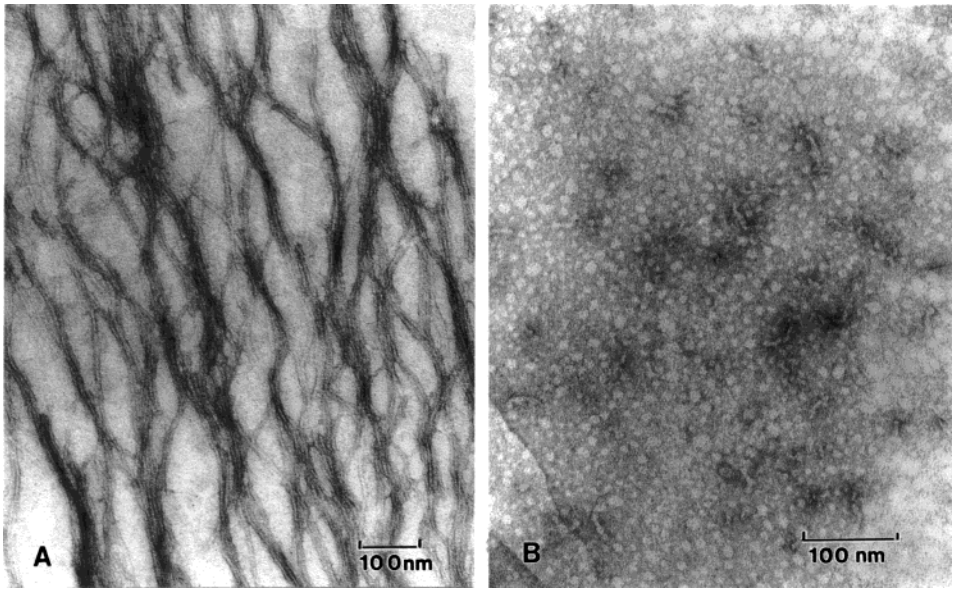

FIGURE 6: Morphology of ABri fibrils and protofibrils. Fibrils and protofibrils were prepared from ABri as described in Experimental Procedures and examined by transmission EM: (A) negatively stained fibrils and (B) negatively stained protofibrils. The scale bars are 100 nm.

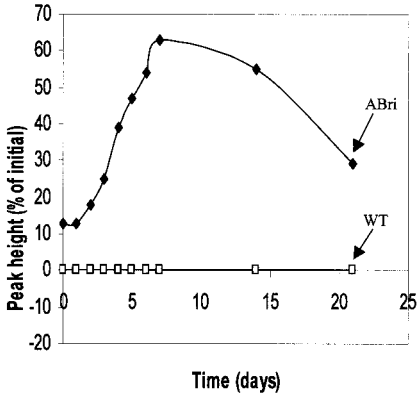

FIGURE 7: Kinetics of ABri polymerization. Freshly prepared WT and ABri (5 mg/mL) solutions in 0.1 M Tris-HCl (pH 9) buffer were incubated for 0, 1, 2, 3, 4, 5, 6, 7, 14, and 21 days and then fractionated by SEC (see Experimental Procedures). Amounts of protofibrils are plotted as a percentage of the dimeric peak level at time zero, which were assigned a value of 100%. Experiments were performed in duplicate.

the pH was increased from 4 to 9, in 0.5 pH unit increments (Figure 8B,C). Over the specified pH range, the β-sheet content of ABri generally increased further after incubation for 24 h (Figure 8B).

FTIR Measurements. The amide I band which is located in the 1615−1695 cm^{-1} region of the spectrum arises primarily due to C═O bond stretching vibrations of the polypeptide backbone (*12*, *24*). This band provides valuable information about the secondary structure adopted by proteins (for recent reviews, see refs *11* and *12*). Figure 8 shows the second-derivative FTIR spectra of ABri and WT peptides (5 mg/mL) suspended in ^2H_2O and incubated for 3 weeks at 37 °C. In Figure 9, the amide I maxima are centered at 1615 and 1617 cm^{-1} for WT and ABri, respectively. Normally intramolecular β-sheet structures exhibit absorbance at higher frequencies, in the 1625−1640 cm^{-1} range. Therefore, the low-frequency (1615−1625 cm^{-1}) bands, seen with peptide and protein aggregates, is suggested to be due to strongly hydrogen bonded intermolecular β-sheets (*12*, *25*, and references therein). The results that were obtained clearly show that both peptides display a predominantly β-sheet structure when they are suspended in an aqueous medium.

A more detailed analysis of the amide I bands in the spectra of the two peptides revealed that the intensity of the intermolecular β-sheet band is greater in ABri than in WT. The intensity differences were evident after calculating the intensity ratio of the intermolecular β-sheet band with respect to other bands in the spectra of the two peptides. It appears that the content of intermolecular β-sheet structure is greater in ABri. Furthermore, the hydrogen bonding characteristics of the intermolecular β-sheet structure, in WT and ABri peptides, appear to be different. This is evident from a shift of the intermolecular β-sheet band from 1615 (WT) to 1617 cm^{-1} (ABri). To conclude, the FTIR results are consistent with a predominantly intermolecular β-sheet structure in both ABri and WT. However, the content of this structure appears to be higher in ABri than in WT. These findings are consistent with CD results.

Molecular Model of ABri. Multiple-alignment secondary structure predictions of uncleaved BRI-encoded proteins (*26*, *27*) predicted a β-strand−turn−strand structure in the 23 N-terminal residues of ABri. This region was modeled in this conformation, with a constraining intramolecular disulfide bond between Cys5 and Cys22 of ABri accommodated in a long β-hairpin (C_5FAIRHFENKFAVETLIC_{22}) stabilized by van der Waals contacts and charge−charge interactions (Figure 10). On the basis of the work of Gunasekaran et al. (*28*), Asn13 and Lys14 are statistically favorable $i + 1$ and $i + 2$ residues of a type I turn in this long disulfide β-hairpin. Further stabilization of this β-hairpin (*15*) was provided by side chain interaction between Glu18 and Arg9 in a non-hydrogen bonding (NHB) position and between Phe11 and Ala16 (in a NHB position) (*15*). The C-terminal sequence of ABri was extended as the third strand of a three-stranded β-sheet, stabilized by van der Waals contacts of NHB pairs, Val17 and Ile30 and Ile21 and Val26 (*15*), and a charge−charge interaction between the carboxy terminus and the Lys14 side chain. To accommodate this third antiparallel

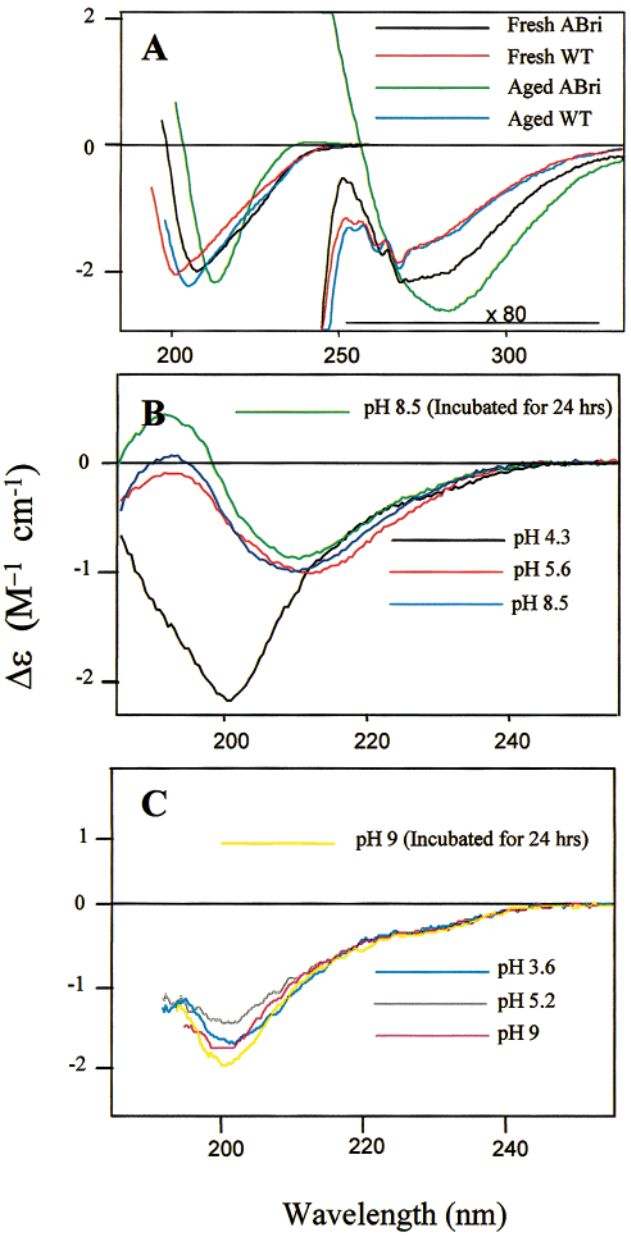

FIGURE 8: CD measurements of ABri and WT solutions. (A) Time-induced changes in the conformation of ABri and WT peptides. CD spectra of ABri or WT at 5 mg/mL in 0.1 M Tris-HCl (pH 9) buffer of either fresh ABri and WT or ABri and WT solutions aged at 37 °C for 3 weeks and then diluted 10-fold with 0.1 mM Tris-HCl (pH 9) buffer just prior to measurement. (B and C) Changes in the conformations of fresh ABri (B) and fresh WT (C) at 0.5 mg/mL in water as a function of pH. The pH titration was carried out in a stepwise manner from pH 4.3 for ABri and pH 3.6 for WT by addition of aliquots of an NaOH solution. The pH was measured just before the spectra were recorded. (B) ABri at pH 4.3, 5.6, 8.5, and 8.5 incubated for 24 h. (C) WT at pH 3.6, 5.2, 7.5, 9, and pH 9 incubated for 24 h.

strand, we placed another type I β-turn at the Cys22-Ser23-Arg24-Thr25 sequence (*29*).

DISCUSSION

Accumulating evidence supports the hypothesis that amyloid fibrillogenesis is a seminal pathogenetic event in neurodegenerative disorders such as Alzheimer's disease, Huntington's disease, prion disease, Parkinson's disease, and dementia with Lewy bodies (reviewed in refs *6*−*8* and *36*).

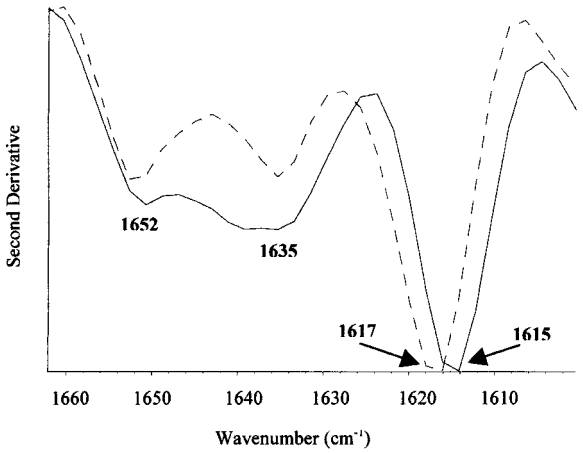

FIGURE 9: FTIR measurements of aged ABri and WT solutions. Spectra were recorded from 5 mg/mL solutions of ABri and WT aged for 3 weeks in 0.1 M Tris-HCl (pH 9) buffer at 37 °C: ABri (− − −) and WT (—).

However, recent studies on amyloid proteins support the idea that nonfibrillar oligomeric species are pathogenic (*23*, *30*−*40*). Studies by us and others have shown that mutant "amyloidogenic" proteins associated with inherited forms of amyloidosis have a greater propensity to form oligomers, including the Aβ peptide in early-onset familial Alzheimer's disease or cerebrovascular amyloidosis (*23*, *30*, *41*), and α-synuclein protein in early-onset familial Parkinson's disease (*38*). Therefore, defining the oligomeric state of the toxic species could be important for developing therapeutics for these amyloidosis disorders (*36*).

In this study, we have compared the oligomerization properties of ABri, the peptide which is deposited in brains of patients with FBD, with the native WT peptide to understand the pathogenic role of the ABri peptide in FBD. Our results showed that fresh or aged solutions of ABri oxidized with an intramolecular disulfide bond contained a series of soluble oligomers, and after incubation for several weeks, higher-molecular weight oligomers containing protofibrils were detected by SEC. In contrast, WT solutions did not contain a series of oligomers, and neither did the reduced form of ABri. Fresh samples of ABri diluted from solution in the disaggregating solvent DMSO or HFIP also showed the presence of oligomers (data not shown). Our results indicate that ABri forms soluble oligomers immediately in fresh solution, whereas oligomers are not formed by WT in solution even after incubation for 3 weeks. Similarly, the highly amyloidogenic Aβ42 peptide, associated with familial early-onset Alzheimer's disease, also forms pathogenic oligomeric species extremely rapidly in solution (*23*, *30*).

Long, intertwined amyloid fibrils of variable length and 5−9 nm in diameter were detected in an aged ABri solution similar in appearance to those found in FBD brains, which showed criss-crossing fibrils ∼10 nm diameter (*42*). In contrast, no fibrils were detected in an aged WT solution. In contrast to our results, previous studies on synthetic ABri, in which the state of oxidation of the disulfide was not characterized, have not shown the formation of elongated amyloid fibrils, whereas the WT peptide has been stated not to produce any insoluble material (*5*).

Kinetic analysis of ABri fibrillogenesis revealed that dimers predominated initially, after which there was a time-

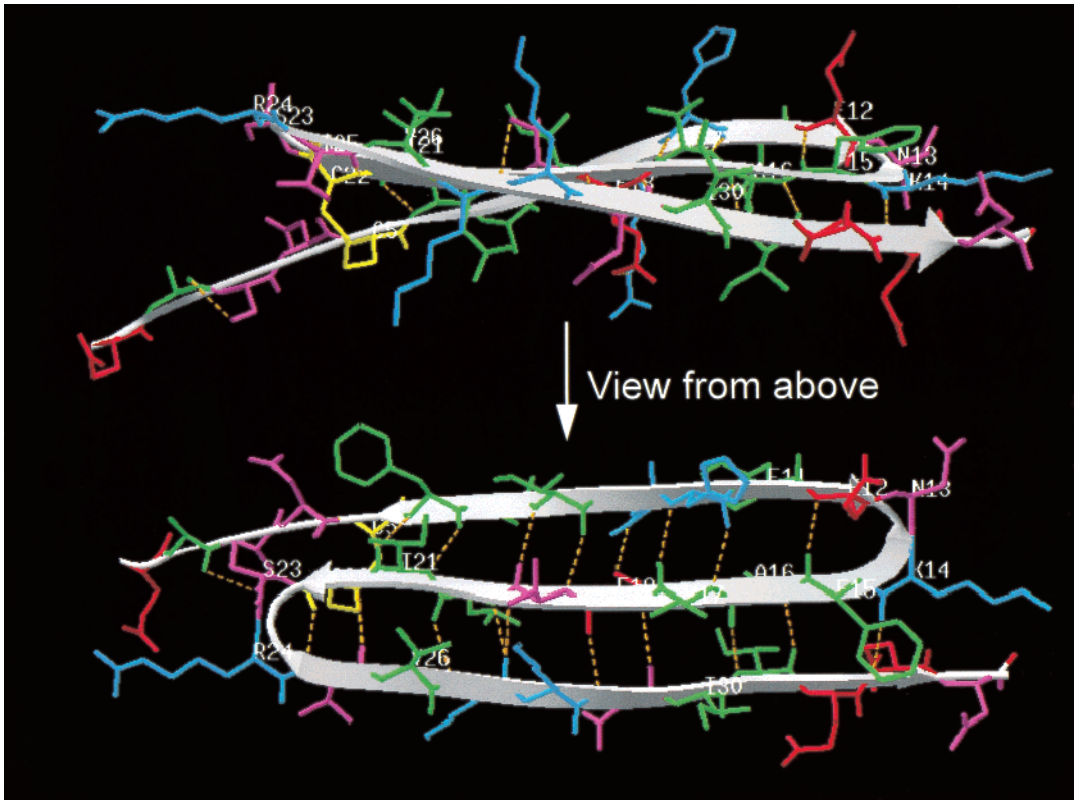

FIGURE 10: Molecular model of ABri. Secondary structure predictions, β-strand register, and β-turn predictions place ABri in a three-stranded β-sheet conformation connected by type I β-turns. This accommodates a constraining intramolecular disulfide bond (yellow) between Cys5 and Cys22 of ABri in an ideal backbone non-hydrogen-bonded position (NHB), allowing the cysteines to adopt the preferred g^+ ($\theta_1 = 300°$) conformation, with an unstrained disulfide torsion angle of ~100° (*15*). Hydrophobic residues are colored green, basic residues blue, acidic residues red, and polar residues pink. Orange dotted lines represent hydrogen bonds. Overall, the β-sheet presents predominantly hydrophobic faces with a central more hydrophilic region, and hydrophilic β-turns, which together could facilitate aggregation.

dependent decrease in dimer levels paralleled by an increase in the extent of protofibril formation. These data are consistent with the protofibrils being an intermediate in ABri fibrillogenesis, resembling the fibrillogenesis of other amyloid proteins such as Aβ and α-synuclein (*22*, *23*, *33*).

CD and FTIR spectroscopy were used to study the conformational preferences of the ABri and WT peptides. Freshly prepared ABri displays a CD spectrum that is consistent with β-sheet structure. In contrast, fresh solutions of WT lacked significant structure. Furthermore, only the ABri solution exhibited the random coil to β-sheet transition when the pH was increased from 4 to 9.

The transition to β-sheet conformation occurring upon aging of WT solutions for 3 weeks was less marked, and the amount of β-sheet in aged WT solutions was smaller than that in aged ABri solutions as observed by CD and FTIR. Changes in the microenvironment of the disulfide and phenylalanine residues were only evident in the aged ABri solution from the analysis of the CD changes in the 250−280 nm region.

Molecular modeling has revealed that a likely structure for ABri is a three-stranded pleated sheet in which the two N-terminal strands are annealed by the disulfide bond. The three-stranded sheet presents a face in which the hydrophobicity is enhanced by the dispositions of the Val and two Ile residues in the C-terminal extension sequence of ABri. The ABri β-sheet model exhibits faces which are predominantly hydrophobic with a central more hydrophilic region on each face. Overall, these features might facilitate aggregation into an amyloid fibril. The decreased hydrophobic contributions from side chain residues of the two-stranded sheet predicted in WT would explain why this peptide does not readily form an oligomeric series beyond the dimer. Recently, another mutation in the BRI gene has been identified in familial Danish dementia (FDD), presenting with neuropathological lesions similar to those associated with FBD (*43*). The BRI mutation in this family produces a larger-than-normal precursor protein, of which the amyloid subunit ADan comprises the last 34 C-terminal amino acids. It has been found that the ADan is the main component of the amyloid deposits in FDD brains (*43*). The ADan peptide has 22 N-terminal residues identical to those of ABri, and similarly contains hydrophobic residues in the C-terminus. These findings support the idea that the C-terminal extensions in ABri and ADan play crucial roles in developing FBD and FDD, respectively. Indeed, our results presented here provide evidence that the disulfide bond and C-terminal extension play important roles in the amyloidogenic properties of ABri. The same could be true for the ADan peptide.

A conformational change to β-sheet has been reported for other amyloid proteins associated with neurodegenerative diseases such as Aβ and NAC in Alzheimer's disease (*10*, *21*, *41*, *44*, *45*), the prion protein in prion diseases (*46*), and the α-synuclein protein in Parkinson's disease (*47*, *48*). Such transitions in secondary structure may well be a general prelude to the formation of toxic oligomeric species by amyloidogenic proteins (for reviews, see refs *6*−*8*). Indeed, in support of this hypothesis, we have found that the WT

peptide is not toxic to neuronal cells, whereas the oxidized form of ABri is toxic.[4]

In summary, we have shown that in solution ABri containing a disulfide bond adopts a β-sheet structure and rapidly forms a series of oligomers. Prolonged aging produces birefringent Congophilic long intertwining fibrils. The dependence of oligomerization and fibril formation in ABri upon the disulfide bond is readily explained by molecular modeling which shows that it anneals a triple-stranded β-sheet in which a hydrophobic face is generated, which is likely to be involved in intramolecular association. It is known that FBD patients carry a mutation in the BRI gene, causing production of ABri. The differences in molecular properties between ABri and WT, and the increased susceptibility of ABri to furin cleavage, explain the association of ABri plaques with neuronal loss in FBD, and are clear examples of the amyloid hypothesis. Hence, understanding the role(s) of ABri in the pathogenesis of FBD may shed light on the cause of dementia in AD as well as in other neurological disorders associated with amyloid deposition.

ACKNOWLEDGMENT

We thank Dr. D. Walsh for insightful advice and critical evaluation of the manuscript.

REFERENCES

1. Worster-Drought, C., Hill, T. R., and McMenemy, W. H. (1933) *J. Neurol. Psychopathol. 14*, 27−34.
2. Plant, G. T., Révész, T., Barnard, R. O., Harding, A. E., and Gautier-Smith, P. C. (1990) *Brain 113*, 721−747.
3. Aikawa, H., Suzuki, K., Iwasaki, Y., and Iiuzuka, R. (1985) *Ann. Neurol. 17*, 297−300.
4. Vidal, R., Frangione, B., Rostagno, A., Mead, S., Révész, T., Plant, G., and Ghiso, J. (1999) *Nature 399*, 776−781.
5. Kim, S. H., Wang, R., Gordon, D. J., Bass, J., Steiner, D. F., Lynn, D. G., Thinakaran, G., Meredith, S. C., and Sisodia, S. S. (1999) *Nat. Neurosci. 11*, 984−988.
6. El-Agnaf, O. M. A., and Irvine, G. B. (2000) *J. Struct. Biol. 130*, 300−309.
7. Johnson, W. G. (2000) *J. Anat. 196*, 609−616.
8. Perutz, M. F. (1999) *Trends Biochem. Sci. 24*, 58−63.
9. El-Agnaf, O. M. A., Goodwin, H., Sheridan, J. M., Frears, E. R., and Austen, B. M. (2000) *Pept. Protein Lett. 7*, 1−8.
10. El-Agnaf, O. M. A., Guthrie, D. J. S., Walsh, D. M., and Irvine, G. B. (1998) *Eur. J. Biochem. 256*, 560−569.
11. Haris, P. I., Lee, D. C., and Chapman, D. (1986) *Biochim. Biophys. Acta 874*, 255−265.
12. Haris, P. I. (2000) *ACS Symp. Ser. 750*, 54−95.
13. Guex, N., and Peitsch, M. C. (1997) *Electrophoresis 18*, 2714−2723.
14. Peterson, S. A., Klabunde, T., Lashuel, H. A., Purkey, H., Sacchettini, J. C., and Kelly, J. W. (1998) *Proc. Natl. Acad. Sci. U.S.A. 95*, 12956−12960.
15. Hutchinson, E. G., Sessions, R. B., Thornton, J. M., and Woolfson, D. N. (1998) *Protein Sci. 11*, 2287−2300.
16. Rodriguez, R., Chinea, G., Lopez, N., Pons, T., and Vriend, G. (1998) *Bioinformatics 14*, 523−528.
17. Hooft, R. W. W., Vriend, G., Sander, C., and Abola, E. E. (1996) *Nature 381*, 272.
18. Ladewig, P. (1945) *Nature 156*, 81.
19. Cooper, J. H. (1974) *Lab. Invest. 31*, 232−238.
20. Elghetany, M. T., and Saleem, A. (1988) *Stain Technol. 63*, 201−212.
21. El-Agnaf, O. M. A., Bodles, A. M., Guthrie, D. J. S., Harriott, P., and Irvine, G. B. (1998) *Eur. J. Biochem. 256*, 560−569.
22. Conway, K. A., Harper, J. D., and Lansbury, P., Jr. (2000) *Biochemistry 39*, 2552−2563.
23. Walsh, D. M., Lomarkin, A., Benedek, G. B., Condron, M. M., and Teplow, D. B. (1997) *J. Biol. Chem. 272*, 22364−22372.
24. Haris, P. I., and Chapman, D. (1992) *Trends Biochem. Sci. 17*, 328−333.
25. Haris, P. I. (1998) *Biosci. Rep. 18*, 299−312.
26. Cuff, J. A., Clamp, M. E., Siddiqui, A. S., Finlay, M., and Barton, G. J. (1998) *Bioinformatics 14*, 892−893.
27. Jones, D. T. (1999) *J. Mol. Biol. 292*, 195−202.
28. Gunasekaran, K., Ramakrishnan, C., and Balaram, P. (1997) *Protein Eng. 10*, 1131−1141.
29. Hutchinson, E. G., and Thornton, J. M. (1994) *Protein Sci. 12*, 2207−2216.
30. El-Agnaf, O. M. A., Mahil, D. S., Patel, B. P., and Austen, B. M. (2000) *Biochem. Biophys. Res. Commun. 273*, 1003−1007.
31. Roher, A. E., Chaney, M. O., Kuo, Y. M., Webster, S. D., Stine, W. B., Haverkamp, L. J., Woods, A. S., Cotter, R. J., Tuohy, J. M., Krafft, G. A., Bonnell, B. S., and Emmerling, M. R. (1996) *J. Biol. Chem. 271*, 20631−20635.
32. Pitschke, M., Prior, R., Haupt, M., and Riesne, D. (1998) *Nat. Med. 4*, 832−834.
33. Walsh, D. M., Hartley, D. M., Kusumoto, Y., Fezouli, Y., Condron, M. M., Lomakin, A., Benedek, G. B., Selkoe, D. J., and Teplow, D. B. (1999) *J. Biol. Chem. 274*, 25945−25952.
34. Hartley, D. M., Walsh, D. M., Ye, C. P., Diehl, T., Vassilev, P. M., Teplow, D. B., and Selkoe, D. J. (1999) *J. Neurosci. 19*, 8876−8884.
35. Harper, J. D., Wong, S. S., Lieber, C. M., and Lansbury, P. T., Jr. (1999) *Biochemistry 38*, 8972−8980.
36. Lansbury, P. T., Jr. (1999) *Proc. Natl. Acad. Sci. U.S.A. 96*, 3342−3344.
37. Saudou, F., Finkbeiner, S., Devys, D., and Greenberg, M. E. (1998) *Cell 271*, 2063−2065.
38. Conway, K. A., Lee, S. J., Rochet, J. C., Ding, T. T., Williamson, R. E., and Lansbury, P., Jr. (2000) *Proc. Natl. Acad. Sci. U.S.A. 97*, 571−576.
39. Bhatia, R., Lin, H., and Lal, R. (2000) *FASEB J. 14*, 1233−1243.
40. Zhu, Y. J., Lin, H., and Lal, R. (2000) *FASEB J. 14*, 1244−1254.
41. Sian, A. K., Frears, E. R., El-Agnaf, O. M. A., Patel, B. P., Manca, M. F., Siligardi, G., Hussain, R., and Austen, B. M. (2000) *Biochem. J. 349*, 299−308.
42. Plant, G. T., Révész, T., Barnard, R. O., Harding, A. E., and Gautier-Smith, P. C. (1990) *Brain 113*, 721−747.
43. Vidal, R., Révész, T., Rostagno, A., Kim, E., Holton, J. L., Bek, T., Bojsen-Moller, M., Braendgaard, H., Plant, G., Ghiso, J., and Frangione, B. (2000) *Proc. Natl. Acad. Sci. U.S.A. 97*, 4920−4925.
44. El-Agnaf, O. M. A., Irvine, G. B., Fitzpatrick, G., Glass, W. K., and Guthrie, D. J. S. (1998) *Biochem. J. 336*, 419−427.
45. El-Agnaf, O. M. A., Jakes, R., Curran, M. D., Middletone, D., Ingenito, F., Bianchi, E., Pessi, A., Neill, D., and Wallace, A. (1998) *FEBS Lett. 440*, 71−75.
46. Pan, K. M., Baldwin, M., Nguyen, J., Gasset, M., Serban, A., Groth, D., Mehlhorn, I., Huang, Z. W., Fletterick, R. J., Cohen, F. E., and Prusiner, S. B. (1993) *Proc. Natl. Acad. Sci. U.S.A. 90*, 10962−10966.
47. El-Agnaf, O. M. A., Jakes, R., Curran, M. D., and Wallace, A. (1998) *FEBS Lett. 440*, 67−70.
48. Serpell, L. C., Berriman, J., Jakes, R., Goedert, M., and Crowther, R. A. (2000) *Proc. Natl. Acad. Sci. U.S.A. 97*, 4897−4902.

[4] O. M. A. El-Agnaf, S. Nagala, B. P. Patel, and B. M. Austen, manuscript submitted for publication.

BI002287I